Springer

Dear Author:

Please find attached the final pdf file of your contribution, which can be viewed using the Acrobat Reader, version 3.0 or higher. We would kindly like to draw your attention to the fact that copyright law is also valid for electronic products. This means especially that:

- You may print the file and distribute it amongst your colleagues in the scientific community for scientific and/or personal use.

- You may make your article published by Springer-Verlag available on your personal home page provided the source of the published article is cited and Springer-Verlag and/or other owner is mentioned as copyright holder. You are requested to create a link to the published article in Springer's internet service. The link must be accompanied by the following text: "The original publication is available at springerlink.com". Please use the appropriate DOI for the article. Articles disseminated via SpringerLink are indexed, abstracted and referenced by many abstracting and information services, bibliographic networks, subscription agencies, library networks and consortia.

- Without having asked Springer-Verlag for a separate permission your institute/your company is not allowed to place this file on its homepage.

- You may not alter the pdf file, as changes to the published contribution are prohibited by copyright law.

- Please address any queries to the production editor of the journal in question, giving your name, the journal title, volume and first page number.

Yours sincerely,

Springer-Verlag

Climate Dynamics (2004) 23: 353–370
DOI 10.1007/s00382-004-0434-9

A. Timmermann · F. Justino · F.-F. Jin · U. Krebs · H. Goosse

Surface temperature control in the North and tropical Pacific during the last glacial maximum

Received: 3 July 2003 / Accepted: 2 April 2004 / Published online: 29 July 2004

Abstract Based on coupled modelling evidence we argue that topographically-induced modifications of the large-scale atmospheric circulation during the last glacial maximum may have led to a reduction of the westerlies, and a slowdown of the Pacific subtropical gyre as well as to an intensification of the Pacific subtropical cell. These oceanic circulation changes generate an eastern North Pacific warming, an associated cooling in the Kuroshio area, as well as a cooling of the tropical oceans, respectively. The tropical cooling pattern resembles a permanent La Niña state which in turn forces atmospheric teleconnection patterns that lead to an enhancement of the subtropical warming by reduced latent and sensible cooling of the ocean. In addition, the radiative cooling due to atmospheric CO_2 and water vapor reductions imposes a cooling tendency in the tropics and subtropics, thereby intensifying the permanent La Niña conditions. The remote North Pacific response results in a warming tendency of the eastern North Pacific which may level off the effect of the local radiative cooling. Hence, a delicate balance between oceanic circulation changes, remotely induced atmospheric flux anomalies as well local radiative cooling is established which controls the tropical and North Pacific temperature anomalies during the last glacial maximum. Furthermore, we discuss how the aftermath of a Heinrich event may have affected glacial temperatures in the Pacific Ocean.

A. Timmermann (✉) · F. Justino · U. Krebs
IFM-GEOMAR, Leibniz Institut für Meereswissenschaften, Düsternbrooker Weg 20, Kiel, Germany
E-mail: atimmermann@ifm.uni-kiel.de

F.-F. Jin
Department of Meteorology, Florida State University, Tallahassee, USA

H. Goosse
Institut d'Astronomie et de Géophysique G., Lemaitre, Université Catholique de Louvain, Louvain-la-Neuve, Belgium

1 Introduction

CLIMAPs planktonic-foraminifera-based sea surface temperature (SST) reconstructions (CLIMAP 1981) for the last glacial maximum (LGM, about 21,000 years ago) indicate that the glacial subtropical/midlatitudinal North Pacific was probably warmer than today. This finding is, however, not consistent with SST reconstructions which are based on other marine (Lee and Slowey 1999) and terrestrial records from the vicinity of the Hawaiian islands (Porter 1979; Rind and Peteet 1985). An ongoing debate (see e.g. Crowley 2000; Kerr 1995) has not solved this discrepancy. Some scientists (Lee and Slowey 1999) have argued that possibly the low-sedimentation records from the CLIMAP compilation are biased towards warm temperatures due to bioturbation effects. This explanation is plausible but not proven. Recent coupled atmosphere-ocean general circulation model simulations (Shin et al. 2003; Kitoh et al. 2001; Bush and Philander 1998; Kim et al. 2003) of the LGM show also a disagreement in simulated North Pacific temperatures. While Kitoh et al. (2001) simulate a warming of the subtropical Pacific, very much like in the CLIMAP record, Shin et al. (2003); Bush and Philander (1998) and Kim et al. (2003) simulate a homogenous North Pacific cooling for the LGM. Neither the modelling nor the reconstruction studies have converged to a consensus yet. It is very surprising that despite this controversial scientific debate, the physical origin of a potential North Pacific warming has not yet been studied in great detail, to our knowledge. Here we study the physical processes that generate North Pacific temperature anomalies during the LGM. Our study is based on climate model simulations which are performed with the intermediate coupled atmosphere-ocean-sea-ice model ECBILT/CLIO (version 3.0). In Sect. 2 we briefly describe the model and the experimental setup. Section 3 describes the simulated sea surface temperature differences between the LGM and the pre-industrial control simulation and their resemblance to a permanent La

Niña pattern. In Sect. 4 we will explain why the Laurentide ice sheet imposes atmospheric anomalies, that may slow down the subtropical and subpolar gyres within the North Pacific ocean. Section 5 deals with the response of the tropical/subtropical ocean circulation to the imposed wind changes. In Sect. 6 changes in radiative forcing and uncertainties in the climate model sensitivities to CO_2 perturbations are discussed. Section 7 studies the effect of glacial meltwater pulses in the North Atlantic, such as the Heinrich 2 event on the temperatures Pacific ocean. The work is concluded with a discussion and summary.

2 Description of the coupled model and the sensitivity experiments

The atmospheric component ECBILT (Opsteegh et al. 1998) of our coupled model is a three layer model with a quasi-geostrophic adiabatic core (Marshall and Molteni 1993) and a set of physical parametrizations for the hydrological cycle (Held and Suarez 1978; Opsteegh et al. 1998) and a partly linearized radiation code. It runs in T21 triangular truncation, which corresponds to an approximate resolution of 5.6° in both latitude and longitude. The coupled ocean-sea ice model CLIO (Goosse et al. 1999, 2002; Goosse and Fichefet 1999) is based on the primitive equations using a free surface and thermodynamic/dynamic assumptions, respectively. A parameterization of vertical mixing (Goosse et al. 1999) is used that represents a simplification of the Mellor and Yamada (1982) 2.5-level turbulence closure scheme. Furthermore, the ocean model CLIO includes mixing along isopycnals and it captures the effect of meso-scale eddies on the transport (Gent and McWilliams 1990) as well as the dense water flow down topographic features (Campin and Goosse 1999). The horizontal resolution of CLIO is 3° and there are 20 unevenly spaced vertical levels in the ocean. The individual models are coupled by exchanging momentum, freshwater and heat. (The coupled model can be down loaded from http://www.knmi.nl/onderzk/CKO/cgi-bin/getfile.cgi?emic.tar.gz). The simulations are performed with weak freshwater flux corrections which mostly affect the North Atlantic region.

Figure 1 shows a comparison between the simulated annual mean near-surface temperature field at 1000 hPa and the "observed" temperature pattern obtained from the Jones (1994) climatology. The simulated global mean near-surface model temperature (14.3 °C) differs from the observations (15.5 °C) by 1.2 °C. Note also that the Jones (1994) temperature compilation represents present-day climate, rather than pre-industrial conditions. Stronger local differences between model simulation and observations can be found in the Pacific cold tongue area, Antarctica and around topographical features, such as the Tibetan Plateau and Greenland. The relative weakness of the trade winds leads to the establishment of a zonally symmetric temperature structure in the tropical oceans. Warm pool temperatures in the Pacific are hence underestimated and cold tongue temperatures are somewhat warmer than observed. The underestimation of the 2 m air temperatures in mountainous areas is most pronounced in seasons of partial snow coverage (not shown). The largest differences between the model and observations occur however north of 65°N. This deficiancy can be partly attributed to an overestimation of the sea-ice thickness and systematic errors in the simulated wind field over the arctic ocean. As can be seen from Fig. 1 the simulated precipitation structure is quite realistic in comparison with the Oberhuber (1988) climatology. However, the amplitude of the simulated precipitation in the ITCZ is strongly underestimated. Given the simplicity of our physical paramterizations, the overall performance is satisfactory and compares with some coarse-resolution coupled general circulation models.

In comparison with a pre-industrial control run which employs an atmospheric CO_2 concentration of 280 ppm, the LGM simulation performed here utilizes the Peltier (1994) ice-sheet topography, an ice sheet-albedo mask, reduced CO_2 concentrations (200 ppm), modified orbital forcing and a LGM vegetation index (Crowley and Baum 1997) for which the deforested soils and plant cover are replaced by their respective glacial albedo. The inclusion of the ice sheet increases the albedo by more than 60% in North America and Europe. When averaged globally the land albedo in the LGM simulation is 7% higher than in the CTR case. The ice-sheet orography is included as an anomaly between the Peltier (1994) ICE-4G reconstruction and present-day orography. This anomaly field is added to the default orography pattern of the atmospheric model ECBILT. The associated changes of the river run-off have not been included here.

Based on previous experiences made with coupled LGM simulations (Liu personal communication) we disregard the role of sea-level changes, and ice sheet runoff in our simulation. In addition, the simplified radiation scheme of ECBILT has been validated for LGM background conditions (N. Weber personal communication). Both, the control and LGM model were integrated for 400 years starting from the same ocean initial conditions which are obtained from a coupled pre-industrial control simulation. Our analysis focuses on the last 100 years, which are characterized by an equilibrated response in the Pacific and some weak trends, in particular in the deep ocean and in the North Atlantic. A detailed description of the simulated changes in the North Atlantic area using an earlier version of this model will be presented elsewhere. The results discussed here depend very little on the oceanic initial conditions.

Some limitations of our modelling approach originate from the set-up of the atmospheric model, which is based on the quasi-geostrophic (QG) approximation and uses just three atmospheric layers. Strictly speaking the QG assumption holds for low Rossby numbers and for small topographic gradients. Despite this theoretical

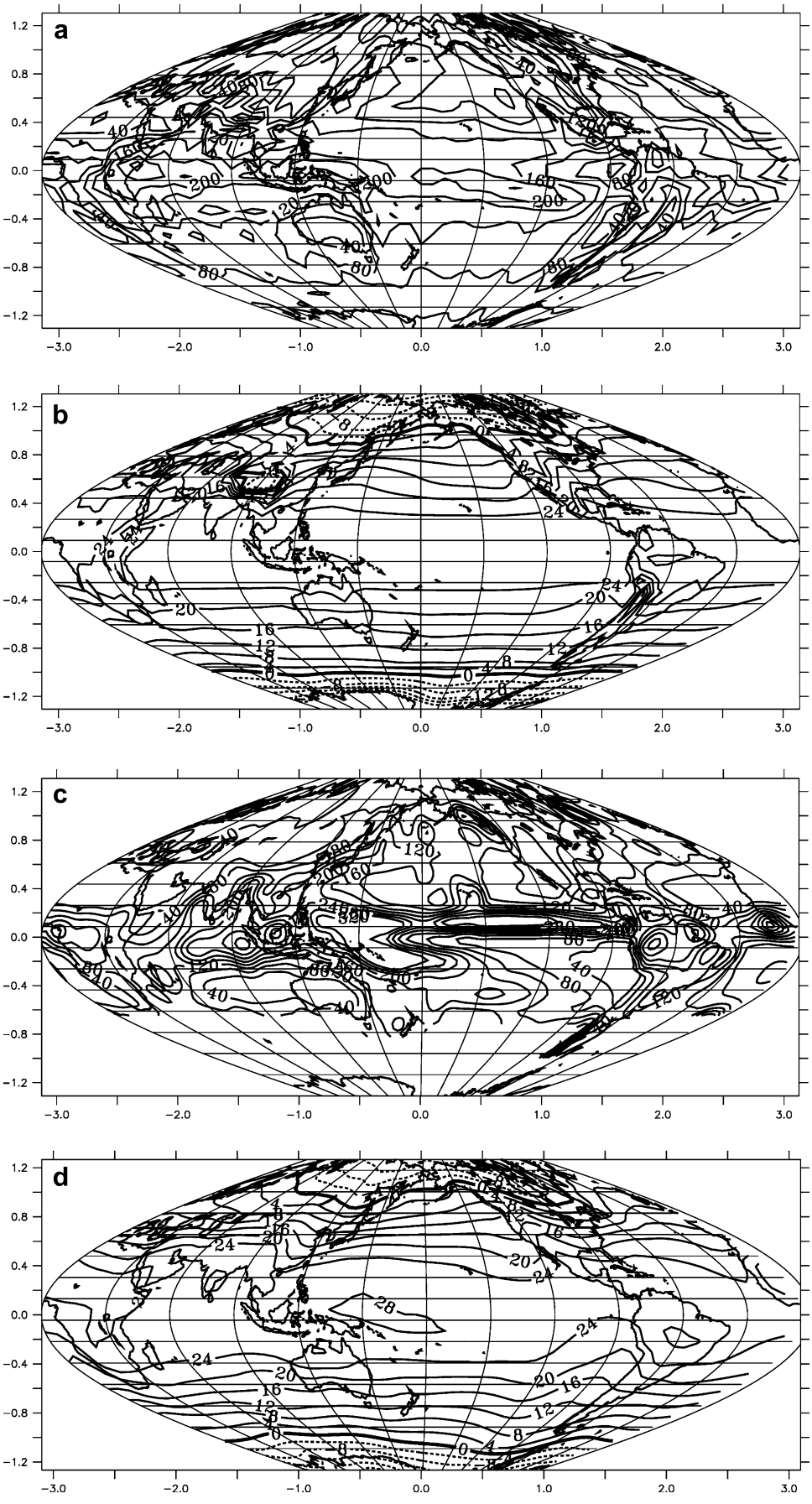

Fig. 1 **a** Simulated precipitation (cm/year) for the pre-industrial control run. **b** Simulated mean near-surface air temperature distribution (°C) for the pre-industrial control run. **c** Observed precipitation pattern [cm/year] from the Oberhuber (1988) climatology **d** Mean surface air temperature distribution ° C from the Jones (1994) climatology dataset.

limitation, we have found (as will be shown later) that the atmospheric response to tropical SST anomalies is qualitatively well captured. However, the amplitude of the response is diminished in comparison with high-resolution primitive equation models, which is mostly due to the low resolution of our model, rather than due to the QG assumption. Furthermore, we have found that the inclusion of topography leads to an improved atmospheric circulation and stationary and transient wave activity as compared to a simulation which neglects orographic forcing. Hence, practically the model can cope much better both with tropical and orographic forcing than the strict theoretical considerations suggest. Furthermore, the inclusion of the Laurentide ice sheet in a three-layer atmosphere (200, 500, 800 hPa) may be problematic. However, a comparison with other coupled LGM simulations reveals that our modelling results compare well with those obtained from primitive equation multi-layer models (as will be shown in more detail later). In addition, our coarse-resolution model suffers from typical problems of such models, such as sluggish western boundary currents and weak undercurrents.

Figure 2 shows the simulated ocean and global (atmospheric + oceanic) heat transport for the control and LGM experiment. The total heat transport attains maximum values of about 5.5 PW near 30°N, resulting mostly from atmospheric transports. This result is consistent with previous modelling studies (e.g. Shin et al. 2003). During the LGM the total heat transport hardly changes, whereas the oceanic poleward heat transport in the northern and southern hemispheric subtropics exhibits an intensification of up to 0.5 PW during the LGM, due to an enhancement of the subtropical cell transport (as will be shown later). This change is somewhat stronger than in the LGM simulation of Shin et al. (2003) and opposite to that of Kim et al. (2003). In the extratropics however, the simulated difference between LGM and CTR simulation is diminishing with increasing latitude. The enhancement of the poleward oceanic heat transports in the subtropics is expected to lead to an overall cooling of the tropical oceans.

These changes of the oceanic heat transport are generated by changes of the meridional transports (see Fig. 3). We observe that the meridional stream function in the LGM run is quite similar to that of the control run, except for significant changes in the upper ocean thermocline circulation, and in particular in the areas of the subtropical cells. Our results are roughly consistent with the modelling study of Shin et al. (2003) and inconsistent with the latest LGM simulation of Kim et al. (2003). Figure 3 also illustrates that the maximum of the stream function in the LGM has shifted south, suggesting that the main area of North Atlantic deep water formation has also shifted southward. During the LGM simulation the inflow of Antarctic Bottom Water into the North Atlantic region is weakened, as compared to the CTR simulation. Whether these modelling results can be directly compared with available proxy data is questionable, because our simulation is an equilibrium experiment, whereas the thermohaline circulation (THC) of the real LGM is probably in a recovering state from the meltwater pulse Heinrich 2. In general the comparison of stationary and transient behaviour of the THC may lead to misinterpretations. The focus of this study is on LGM climate changes in the tropical and North Pacific.

3 Surface temperature patterns

The global mean surface temperature of the equilibrated LGM simulation is 3.2° lower than for the pre-industrial simulation. The sea-surface temperature anomalies with respect to the pre-industrial simulation are shown in

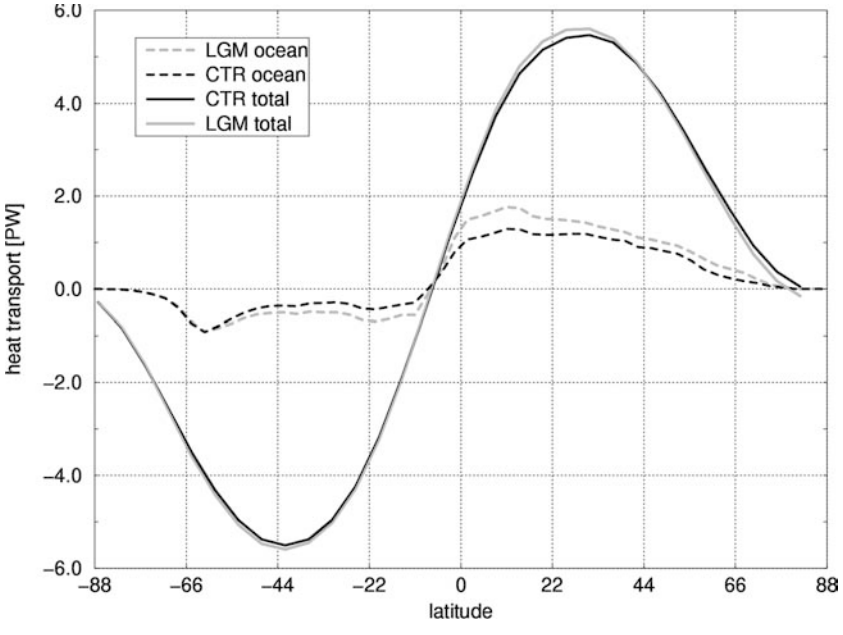

Fig. 2 Time average (years 300–400) of the zonally averaged oceanic (*dashed*) and total (*solid*) heat transport (PW) for the control (*black*) and the LGM (*grey*) simulation

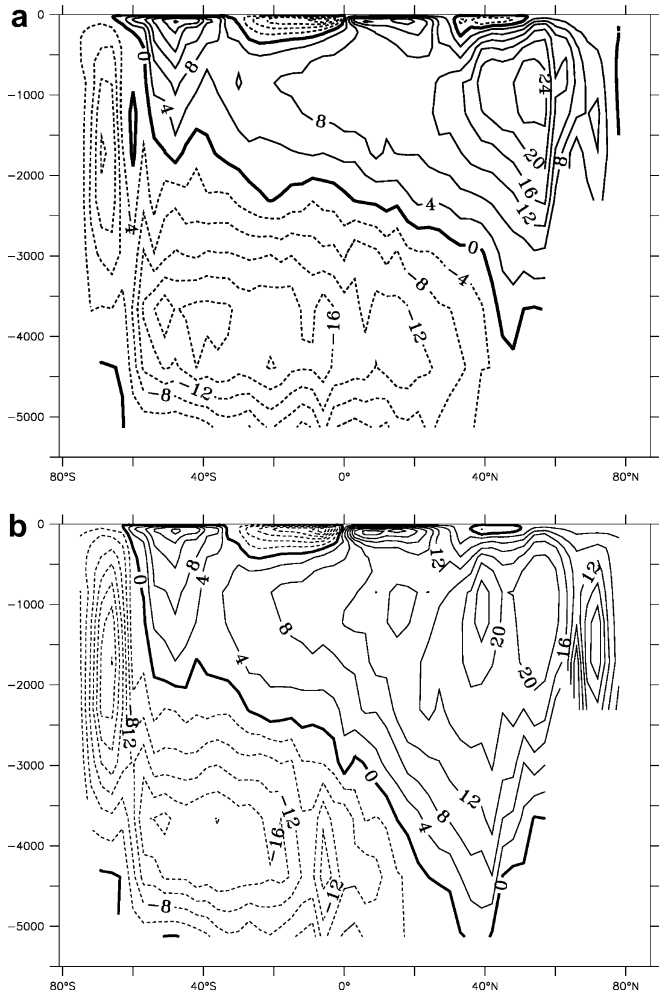

Fig. 3 Time average (years 300–400) of the zonally averaged global stream function (Sv = 10^6 m^3/s) for **a** the control and **b** the LGM simulation

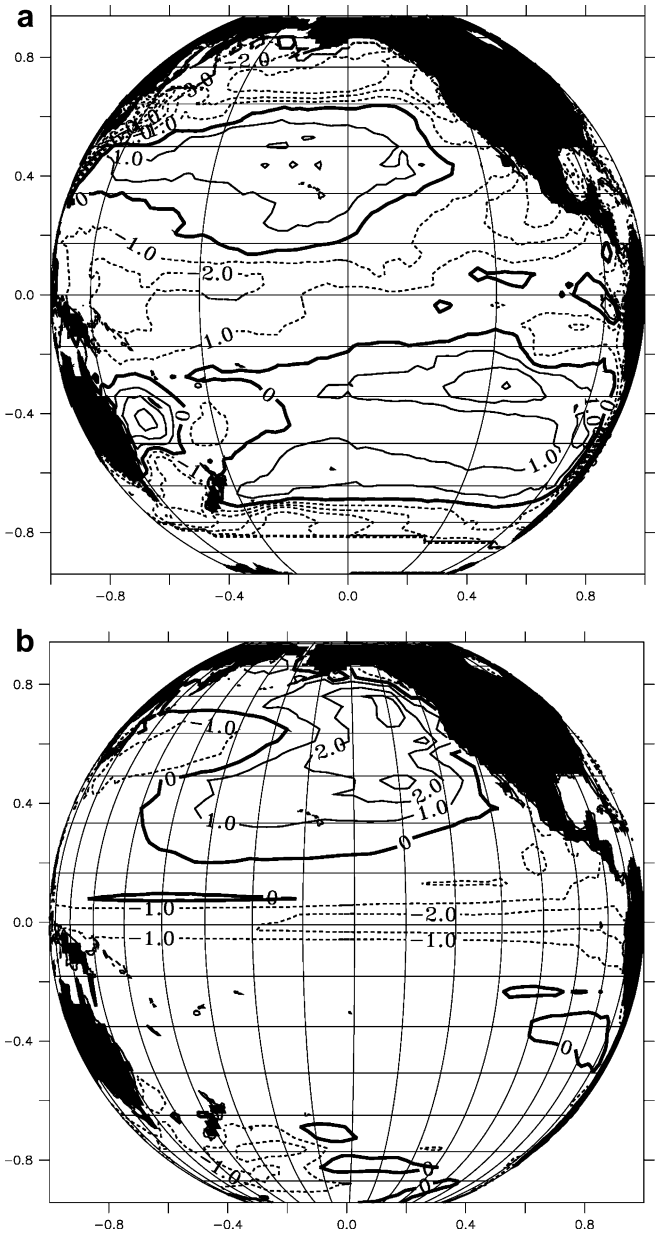

Fig. 4 **a** Sea surface temperature anomalies (K) of the CLIMAP SST reconstruction. **b** Sea surface temperature anomalies (K) computed from the difference between LGM and pre-industrial sea surface temperatures

Fig. 4. We see an annual mean cooling of the tropical oceans by about 2.5 °C. The winter cooling (not shown) amounts to about 3 °C whereas the summer cooling attains values of about 1–2 °C. These estimates agree fairly well with recent reconstructions from the Galapagos Islands by Koutavas et al. (2002), whereas they are weaker than from the reconstructions of Pisias and Mix (1997); Hostetler and Mix (1999); Lea et al. (2000). The most striking feature, however, is the warming of the subtropical and midlatitudinal eastern North Pacific, which also exhibits a strong seasonality (not shown). In the North Pacific our simulated temperature anomaly pattern is somewhat similar to the CLIMAP (1981) reconstruction. The reconstructed warming of the subtropical North Atlantic (Hostetler and Mix 1999) and the subtropical South Pacific (CLIMAP 1981) is not simulated by our coupled atmosphere-ocean-sea ice model under LGM conditions. The simulated characteristic North Pacific warming pattern on the eastern side is opposed by a cooling of the Kuroshio area, like in the CLIMAP SST anomaly record. A comparison with terrestrial tropical/subtropical paleo-data reveals many discrepancies: Instead of a reconstructed cooling of northeastern Brazil by about 5 °C (Stute et al. 1995), our LGM simulation can only account for a 2.5–3 °C cooling (with respect to pre-industrial times). Furthermore, cores taken from submerged corals (Guilderson et al. 1994) suggest a cooling of the Carribean by about 5 °C in contrast to our simulated 1–2 °C surface temperature difference in the tropical/subtropical North Atlantic (not shown). In addition the sea-ice margin of our LGM simulation (not shown) is too far north, as compared to the CLIMAP (1981) and too far south as compared to the most recent GLAMAP reconstructions (Sarnthein et al. 2003) in the northeast Atlantic, (Pflaumann et al.

2003). The sea-ice margin is partly controlled by the relatively low climate sensitivity of our coupled model to CO_2 changes and a rather strong overturning in the northern North Atlantic as will be discussed in forthcoming studies.

Figure 5 displays the simulated precipitation changes between LGM and control simulation. These hydrological changes are consistent with a typical La Niña response in the tropics. Furthermore, the northeast Pacific warming is associated with an increase of precipitation, which reaches also the Californian coast. Lake level reconstruction from California (Kohlfeld and Harrison 2000) support this simulated feature.

Focusing on the Pacific temperature anomalies we see a kind of permanent La Niña pattern (Fig. 4). Similar to a present-day La Niña situation (Lau and Nath 1996) the LGM SST anomaly pattern shows a warming of the eastern North Pacific. In order to further highlight this correspondence with the dynamics of the El Niño-Southern Oscillation (ENSO) phenomenon we computed regression patterns of the interannual Pacific SST anomalies and the Niño 3 SSTA index (SST anomalies averaged from 5°S to 5°N and 150°W to 90°W) derived from our control simulation. The simulated interannual ENSO activity of our coupled model is weak, as can be expected from the low resolution of the model components and the use of quasi-geostrophic atmospheric dynamics. The Niño 3 SSTA standard deviation (0.27 K) is comparable to that of other coupled low-resolution climate models such as the GFDL (Knutson et al. 1997) and the ECHAM3/LSG model (Timmermann et al. 1999). It is important to note that in comparison with Lau and Nath (1996) the pre-industrial teleconnection patterns associated with a 1 K warming of the Niño 3 area have quite a realistic structure (see Fig. 6), given the simplicity of our atmospheric model. However the amplitude of the teleconnection pattern is underestimated by a factor of 1.4 as compared to an R15 atmospheric general circulation model sensitivity experiment (Lau and Nath 1996).

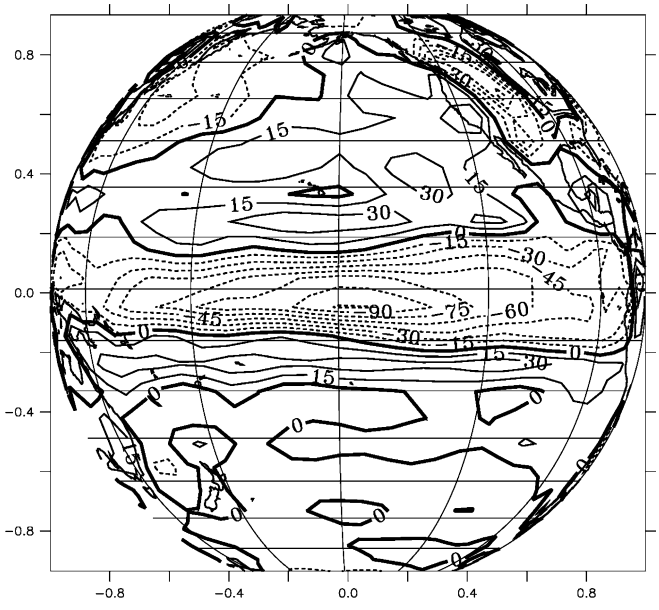

Fig. 5 Simulated precipitation difference (cm/year) between the LGM and the control simulation

The simulated 500 hPa stationary eddy response to a 1 K eastern equatorial warming (cooling) is characterized by a strengthening (weakening) of the Aleutian Low and a PNA-type pattern (see Fig. 6b). Assuming that the stationary teleconnections from the tropical Pacific have the same patterns as the interannual teleconnections we can conclude that for a permanent La Niña state such as during the LGM (opposite to Fig. 6) a reduction of sensible cooling in the central North Pacific can be expected, thereby leading to a warming in that area (similar to the results reported in Lau and Nath 1996). In the northwestern Pacific, however, latent and sensible heat flux anomalies are positive (negative) for an El Niño (La Niña) pattern (Fig. 6c,d), and thus lead to a warming (cooling) of the surface ocean. We have also computed the ENSO teleconnection patterns using the LGM simulation. Although there are regional changes (not shown), the basic conclusions from the control teleconnection patterns are still valid.

An interesting theoretical question to be addressed here is whether a quasigeostrophic coarse-resolution atmospheric model can capture some features of the response to tropical SST anomalies. We perform an atmospheric response experiment with ECBILT which uses present-day climatological SST boundary conditions and an eastern equatorial temperature anomaly characterized by a Niño 3 amplitude of –3.4 °C. The difference between the perturbed and the climatological run is depicted in Fig. 7. The stationary eddy streamfunction represents a strong surface divergence towards the equator and an upper level convergence west of the diabatic heating source. This highly baroclinic anomalous circulation pattern reflects the stationary Kelvin wave response to the east of the forcing and the stationary Rossby wave response to the west of the heat source. In comparison with a T106 ECHAM4 response experiment (U. Merkel private communication) the pattern of our simulated stream function response pattern looks qualitatively quite realistic. However, the amplitude of our response is underestimated by a factor of 2–3. Part of this underrepresentation can be attributed to the quasi-geostrophic formulation of our atmospheric model, partly to the coarse-resolution (T21).

4 Topographically induced wind patterns

The response of the atmospheric circulation to topographic barriers, such as the Laurentide ice sheet has been studied extensively (see e.g. Cook and Held 1988; Rind 1987). The main conclusion which can be drawn from these studies is that an upper-level downstream blocking situation establishes over the North Pacific, Alaska and Northern Canada in response to the Lau-

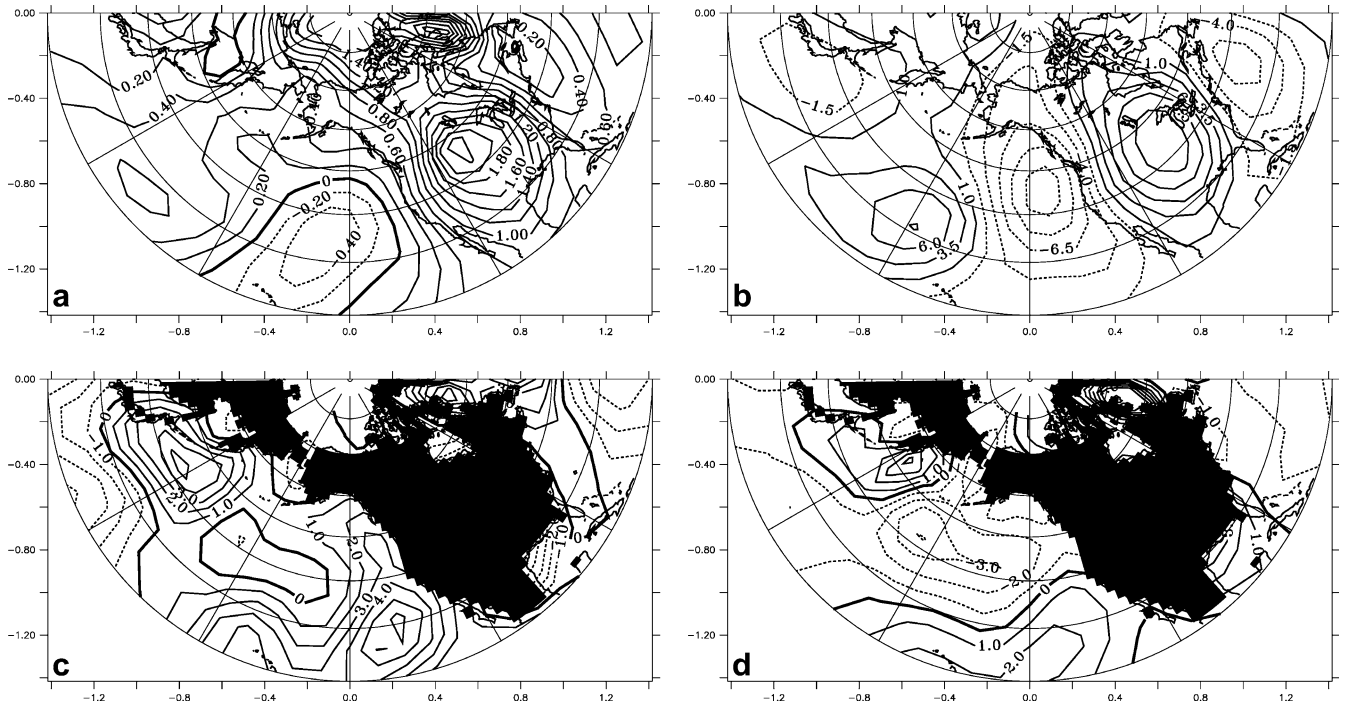

Fig. 6 **a** Annual surface temperature anomalies (K/K) regressed upon the Niño 3 SSTA index for the control simulation. **b** Stationary eddy geopotential height anomalies at 500 hPa (m/K) regressed upon the Niño 3 SSTA index for the control simulation. **c** Latent heat flux anomalies at ($W/m^2/K$) regressed upon the Niño 3 SSTA index for the control simulation. **d** Sensible heat flux anomalies ($W/m^2/K$) regressed upon the Niño 3 SSTA index for the control simulation

rentide ice sheet. The meridional velocity anomalies v', induced by the topographic forcing can be computed from the thermodynamic and continuity equations as follows (Cook and Held 1988):

$$v' \sim -\frac{\bar{u}}{\cos\phi}\frac{\partial h}{\partial \lambda}\frac{\partial \bar{\Theta}/\partial z}{\partial \bar{\Theta}/\partial \phi} \ . \qquad (1)$$

v' is proportional to the zonal mean wind $\bar{u}$and the zonal topographic gradient $\frac{\partial h}{\partial \lambda}$. The third term represents the slope of an isentropic surface and can be computed from the zonally averaged static stability $\partial\bar{\Theta}/\partial z$and the meridional zonally averaged temperature gradient. A westerly mean circulation $\bar{u} > 0$, which is also modulated by the annual cycle (large $\bar{u}$in boreal winter and weak $\bar{u}$in boreal summer), imposes negative meridional wind anomalies in the North Pacific due to the topographic barrier $\frac{\partial h}{\partial \lambda} > 0$of the Laurentide ice sheet. During the LGM the static stability of the atmosphere is enhanced, thereby further enhancing the southerly flow anomaly on the western side of the orographic anomaly. The absolute value of the zonally averaged meridional temperature gradient $\partial\bar{\Theta}/\partial\phi$increases also during the LGM, thereby reducing the topographically induced flow anomalies. We also expect that a downstream low as generated by the Laurentide ice sheet interacts with an upstream high triggered by the Eurasian ice sheet. This may lead to a more complicated flow situation over the North Atlantic. These predicted dynamical features can be found in our simulation: The simulated northern hemispheric surface stationary wave anomaly patterns between LGM and control simulation are depicted in Fig. 8 for the 200 and 800 hPa geopotential height surfaces. In 200 hPa the atmospheric response traces the meridional anomalies predicted by Eq. (1): southward anomalies on the western sides of the ice sheets, associated with upstream high pressure and northward anomalies and low-pressure anomalies on the downstream side of the Laurentide and Eurasian ice sheets.

Our simulated seasonal (not shown) and annual mean (Fig. 8) stationary wave anomalies induced by LGM forcing are qualitatively and quantitatively very similar to those obtained by Kitoh et al. (2001). The same holds also for the simulated SST structure. The upstream high and downstream orographic low features of the ice-sheets are also well reproduced by Rind (1987) their Fig. 22, Broccoli and Manabe (1987). The results of Shin et al. (2003) their Fig. 16b, also show a near-surface wind response which is similar to ours, both qualitatively and quantitatively. It should be noted that in our simulation also the extratropical atmospheric response to the permanent La Niña state contributes about 10–20% to the amplitude of the stationary wave pattern. The Pacific bipolar anomaly pattern in Fig. 8 is associated with a weakening of the jet stream in the Pacific area, with possible consequences for the wind-driven ocean circulation, as will be documented later. Furthermore, the 800 hPa stationary wave pattern exhibits a decrease of the Siberian high and a distortion of the

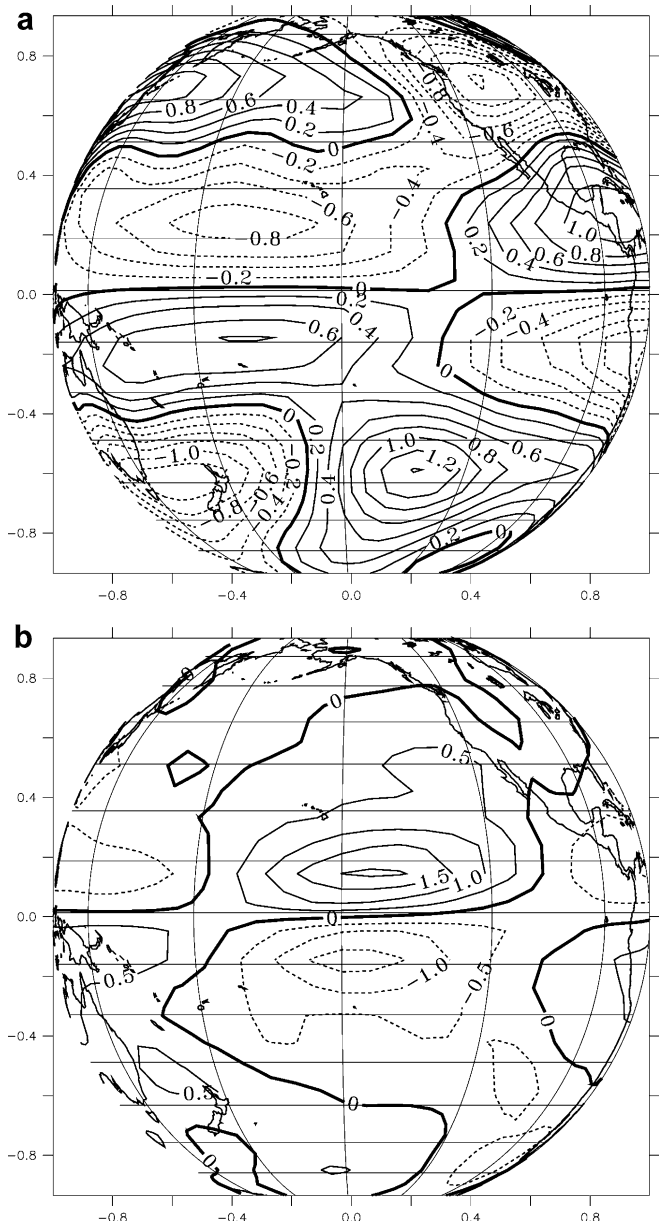

Fig. 7 **a** The 200 hPa and **b** 800 hPa eddy stream function response pattern (10^6 m^2/s) to a –3.4 degree Niño3 eastern equatorial Pacific surface temperature anomaly. The simulation is performed using pre-industrial conditions

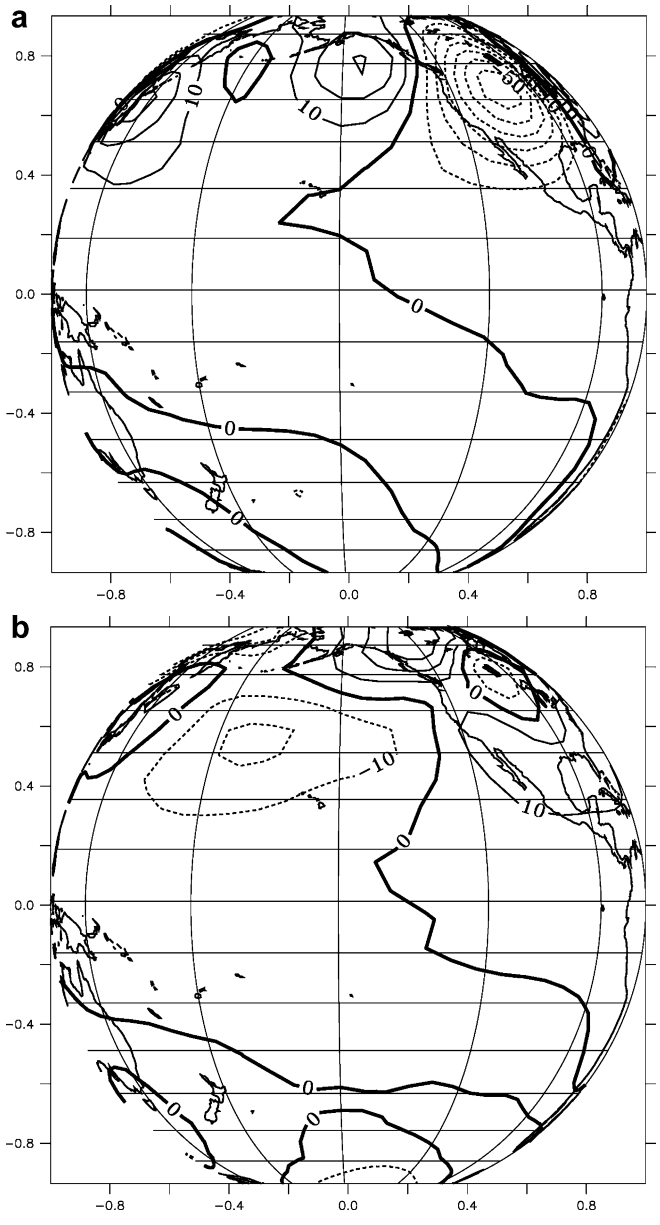

Fig. 8 Annual mean eddy geopotential height difference (m) between LGM and pre-industrial simulation **a** at 200 hPa and **b** at 800 hPa

Tibetan wave, in accordance with previous model results (Broccoli and Manabe 1987) (not shown).

These large-scale changes of the atmospheric circulation are associated with large-scale shifts of the snowfall patterns (not shown). More snow (400 m/1000 years) falls over the central Laurentide and the Scandinavian ice sheets. Hence the simulated orographic influence of the ice-sheet height on the global atmospheric circulation patterns provides a positive feedback for the glacial climate system.

In addition to changes in the stationary waves one may also expect modifications in the transient wave activity. As shown in Fig. 4 the northern North Pacific warms by several degrees which leads also to a reduction of the North Pacific sea-ice extent. These changes weaken the baroclinic conditions in the atmosphere and hence the thermal wind and subsequently the transient eddy activity. A measure for the baroclinicity is the baroclinic eddy production rate of transient eddies (2–8 day band-pass filtered daily data). In Fig. 9 we see that the baroclinic eddy production rate in the northwestern Pacific is significantly smaller than during the control simulation. The simulated reduction of the baroclinic eddy production in the Pacific jet entrance region can be explained by larger vertical and weaker meridional temperature gradients in the atmosphere, which are associated with changes in the static stability

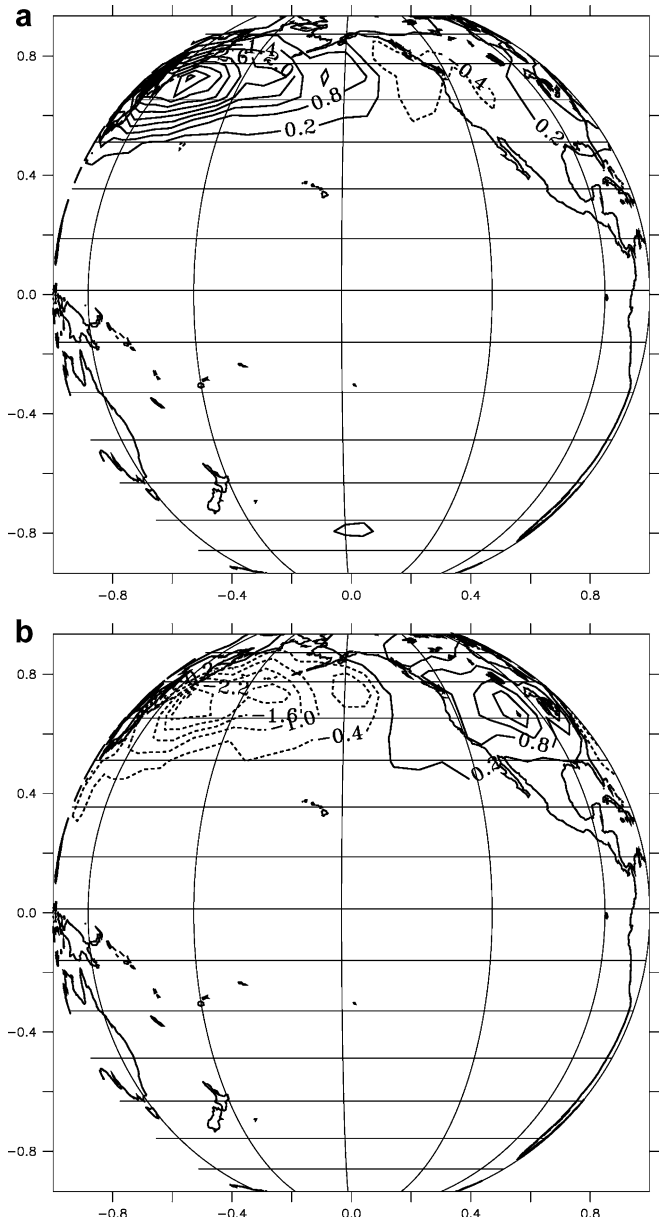

Fig. 9 **a** Baroclinic eddy production rate at 500 hPa (10^{-4} m^2/s^2) averaged over the boreal winter season for the pre-industrial simulation. **b** Difference between baroclinic eddy production rate of the LGM and the CTR simulation

and the vertical velocity shear, respectively. Associated changes in the eddy kinetic energy and the poleward temperature flux due to transient eddies (not shown) are in accordance with the simulated reduced baroclinicity in the North Pacific region.

In order to understand the changes of the mean zonal atmospheric circulation, we study the role of total eddy momentum fluxes, which have the potential to accelarate or decelarate zonal circulations and induce secondary meridional circulation anomalies. The total (transient and stationary) eddy momentum flux and its divergence are displayed in Fig. 10. One observes a strong upper-level anomaly at a latitude of about 40°N which can be attributed to the orographically forced stationary eddy momentum flux anomalies. The meridional gradient of the total eddy momentum fluxes which drives secondary meridional circulations (Kuo 1956) is highest in the subtropics (Fig. 10) between 25–35°N. This upper-level convergence induces deceleration of the upper level westerlies (Fig. 11) as well as a clockwise circulation with ascending motion at about 15–25°N and descending motion at 30–45°N. These vertical velocity anomalies are well captured by the omega field (Fig. 11) at 350 hPa. In turn the anomalous vertical motions generate pressure anomalies: a surface high pressure anomaly between 28–42°N and a low presure anomaly between 20 and 28°N. As a result of near-geostrophic balance between pressure gradient and trade winds the steepened pressure gradient between subtropics and tropics generates stronger easterlies (see Fig. 11). The mechanism is similar to the one suggested by Bush (2001). In addition, the associated temperature anomalies (see later) in turn reinforce the equatorial changes of the trade winds via the coupled atmosphere-ocean instability (Bjerknes 1969). As suggested by A. Bush (personal communication 2003) the intensification of the easterlies is partly driven by atmospheric changes, due to the glacial boundary conditions, partly maintained by coupled atmosphere-ocean instabilities.

It is this intensification of the trade winds which drives changes in the ocean circulation in the subtropical Pacific as will be shown later.

5 Spin-down of the subtropical gyre, intensification of subtropical cell

Sensitivity experiments focusing on the separate roles of ice albedo, orography, CO_2 reduction and vegetation have shown that the mean wind changes over the North Pacific can be explained to a large extent in terms of topographic forcing, as proposed already. In the present framework, it is interesting to analyze the consequences of an altered atmospheric circulation for the wind-driven ocean circulation in the North Pacific. Figure 12 depicts the mean surface velocities and the simulated surface velocity changes during the LGM. As compared to reality, the front that separates the subtropical and the subpolar gyre is positioned too far northward in our coupled model simulation. For the LGM one observes a reduction of the subtropical gyre, which can be directly attributed to a reduction of the wind-stress curl in the North Pacific, and hence due to a reduced Sverdrup transport. The reduction of the subtropical gyre by about 30 Sv is expected to result in a cooling within the Kuroshio area and a warming in the eastern North Pacific, in accordance with Fig. 4.

Furthermore, in the LGM simulation we observe also a strong intensification of the tropical current system. The intensified South Equatorial current transports colder waters to the warm pool area. In addition stronger surface current divergence as documented in

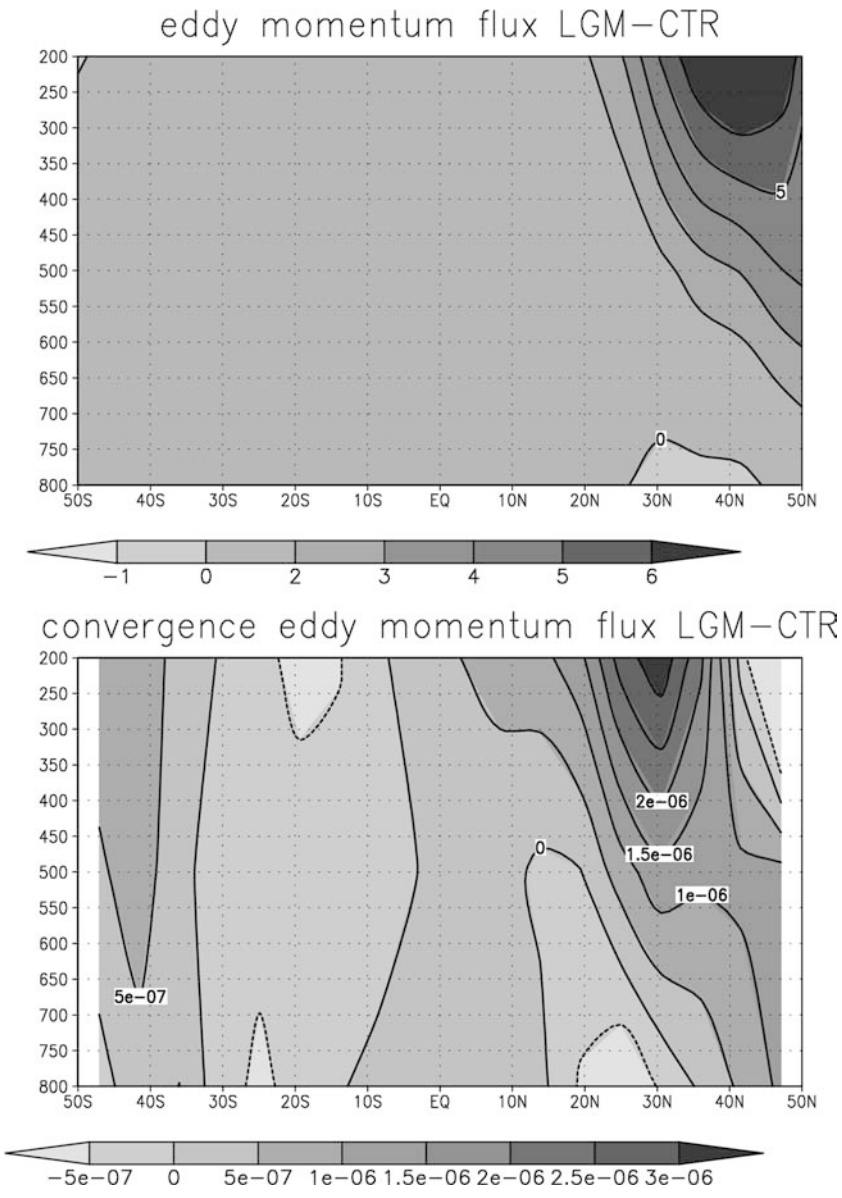

Fig. 10 **a** Transient plus stationary eddy momentum flux difference (m^2/s^2) between LGM and CTR simulation. **b** Meridional derivative of the eddy momentum flux anomaly (LGM-CTR)

Fig. 12 will lead to an enhanced upwelling in the eastern equatorial Pacific.

A substantial amount of tropical heat is carried poleward by the subtropical cells (McCreary and Lu 1994). The strength of these meridional circulation cells as well as the magnitude of equatorial upwelling and the equatorial undercurrent can be easily modified by imposing subtropical windstress anomalies (Liu and Philander 1995; Klinger et al. 2002). As the strength of these cells is strongly determined by the zonally averaged windstress and the Coriolis parameter (the total Ekman transport) in the subtropics (McCreary and Lu 1994) we expect that the trade wind intensification described above will lead to a spin-up of these meridional cells. It was shown in (Liu and Philander 1995 and Klinger et al. 2002) that a trade wind intensification of 30–50% leads to an enhancement of the meridional transports by about 2 Sv (1 Sv = 10^6 m/s) and an equatorial cooling of about 1–2 °C. Trade wind changes, driven by the glacial boundary conditions are of similar magnitude than in the sensitivity experiments of Liu and Philander (1995) and Klinger et al. (2002). The resulting changes in the meridional transport are about 2–4 Sv (Fig. 13) (It should be noted here that, despite the simplified physics of the atmospheric model, the strength of the equatorial upwelling, 38 Sv, as derived from the meridional stream function is similar to the strength as simulated by a forced ocean model simulation, using realistic wind data). This effect as well as the cooling of the tropical oceans by about 2 °C are in accordance with the modelling results mentioned. In turn the permanent La Niña state in the tropical Pacific drives stronger equatorial trade winds due to the Bjerknes feedback (Bjerknes 1969). Despite the quasi-geostrophic approximation used in the atmospheric model the overall wind-response pattern to eastern equatorial temperature anomalies is

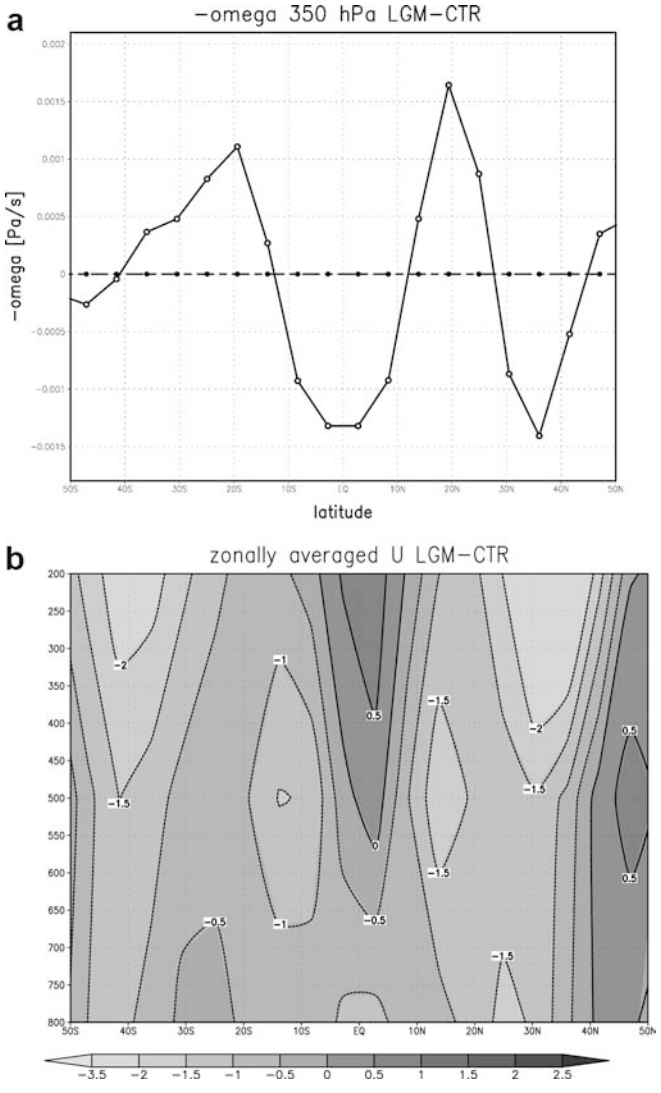

Fig. 11 **a** Zonally averaged negative vertical wind pressure ω difference between LGM and CTR simulation (Pa/s). *Negative values* indicate descending motion, *positive values* ascending motion. **b** Zonally averaged zonal wind anomalies (LGM-CTR) (m/s)

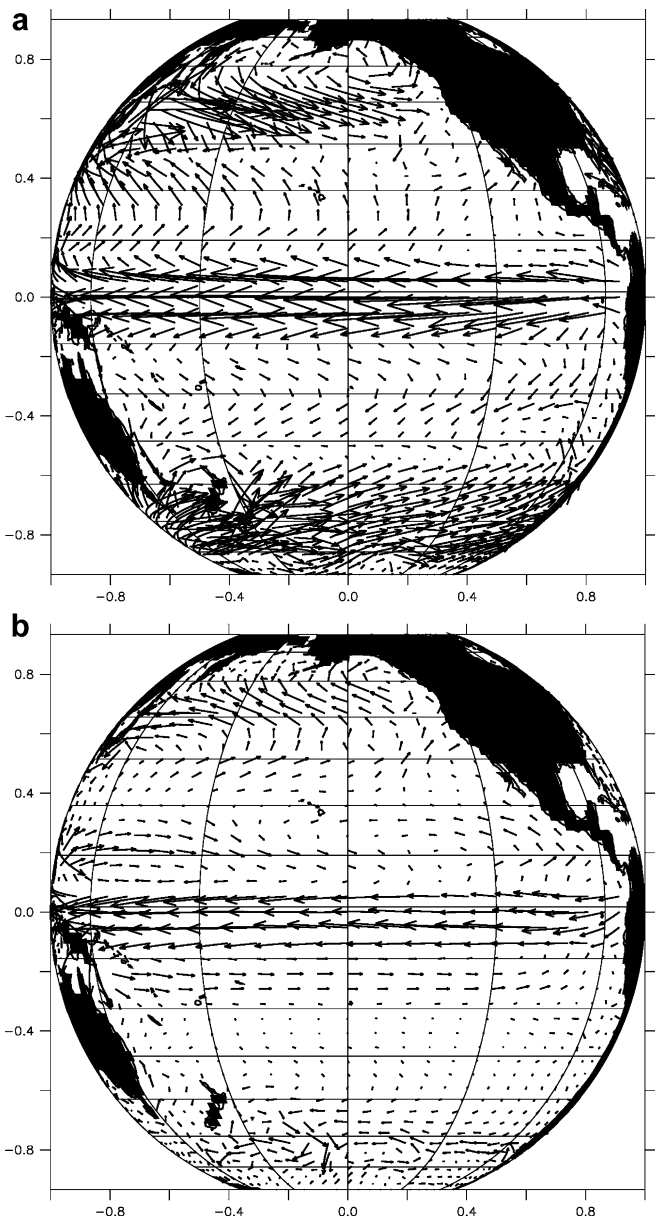

Fig. 12 **a** Simulated surface current (CTR) **b** Surface current anomalies between the coupled LGM experiment and the CTR run

quite realistic as has been checked in a series of sensitivity experiments. However, the amplitude of the Bjerknes response is underestimated by a factor of 2–3. A strengthening of the subtropical cells leads also to an intensified poleward surface heat transport, thereby warming up the subtropical Pacific. This is further illustrated in Fig. 14 showing the anomalous ocean dynamical heating and the total heat flux change between LGM and control simulation. The enhanced northern subtropical cell leads to an enhanced north eastward surface transport of warm pool waters into the subtropical Pacific. The associated horizontal temperature advection leads to slight warming (0.2 K/month) of the western and central subtropical Pacific. The weakening of the subtropical gyre manifests itself in a cooling tendency of the Kuroshio area by about –0.3 K/month. The supply of cold waters from the subpolar area is diminished in the eastern North Pacific due to the weakened subtropical gyre, thereby generating a warming of the eastern North Pacific (Fig. 14) of about 0.5 K/month, in accordance with Fig. 4. In a recent study of Liu et al. (2002) the importance of ocean dynamic heating for the generation of a cold eastern equatorial Pacific has also been highlighted. The net atmosphere-ocean heat flux is also contributing to the surface temperature anomalies in the tropical and North Pacific. As can be seen from Fig. 14, lower panel, the southern subtropical gyre area exhibits a warming tendency of about 0.2 K/month, whereas the northeastern Pacific experiences a cooling due to enhanced cold air advection (sensible heat flux anomalies) during the LGM. Thus, the southern part of the North Pacific warming (Fig. 4)

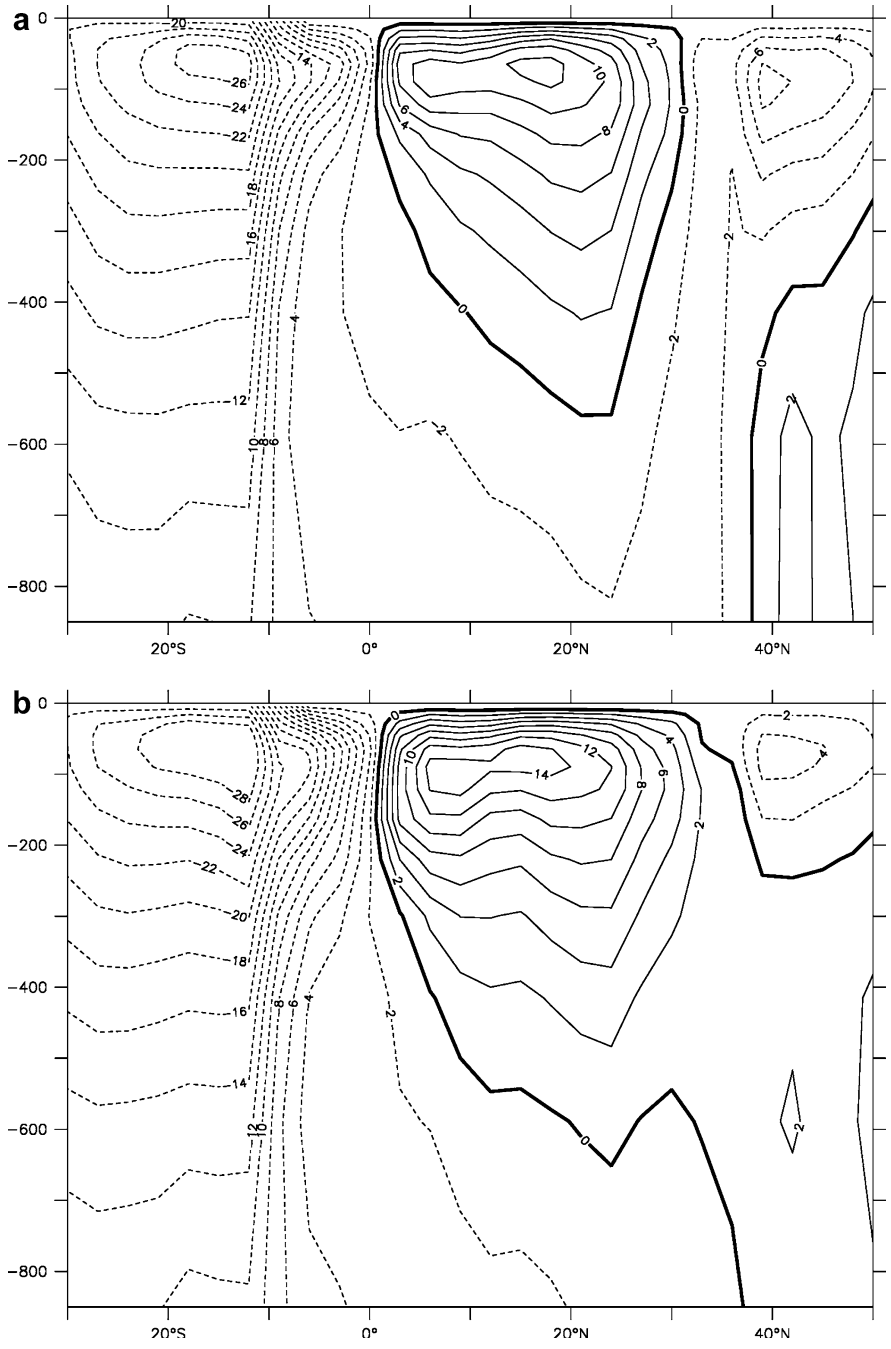

Fig. 13 **a** Zonally integrated stream function (Sv) in the Pacific basin for the CTR experiment; **b** as **a** but for the LGM simulation

originates from air-sea flux anomalies (mostly latent and sensible heat flux anomalies), whereas the northern part is generated by lateral ocean dynamical changes, which outweigh the local air-sea fluxes in that area. The air-sea flux anomalies in the eastern equatorial Pacific clearly show the typical damping effect as a response to the permanent La Niña anomaly.

6 Climate sensitivity

In order to assess the role of CO_2 forcing on changing the magnitude of the tropical/extratropical Pacific dipole we performed an additional experiment in which the atmospheric CO_2 concentration is reduced to 100 ppm. This experiment, despite its unrealistic greenhouse gas concentration, mimicks the uncertainty in the climate sensitivity (Houghton et al. 2001) in a very crude manner. The results clearly show a global cooling of the oceans (not shown). Sea-ice margins have extended much farther equatorward. The tropical oceans cool by about 3–5 °C. In spite of the overall cooling tendency the eastern North Pacific shows little cooling and in some places even a slight warming. This is mainly due to the ocean dynamical effects described above and the remote La Niña-type response, which counteract the radiative cooling locally.

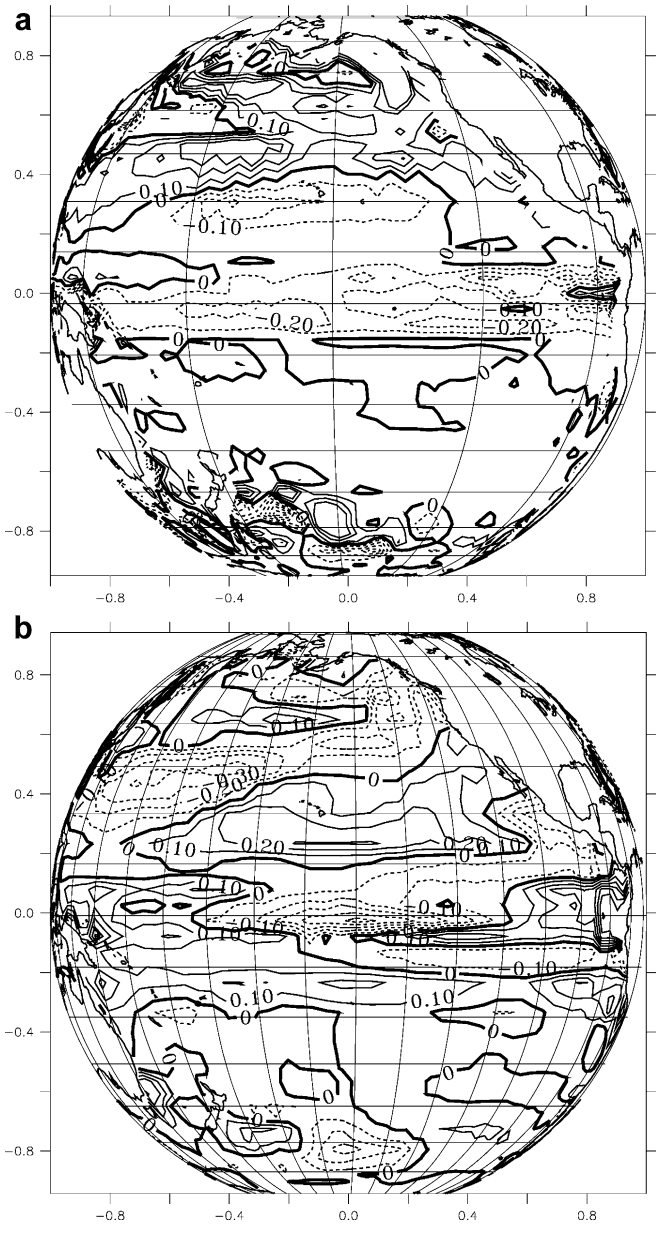

Fig. 14 **a** Change of lateral dynamical heating rates (K/month) between LGM and pre-industrial simulation. **b** Change of net heat atmosphere-ocean heat flux (K/month). Positive values indicate a warming tendency

More sensitivity experiments are performed in order to quantify the relative roles of CO_2 changes and dynamical changes due to orographic forcing on the tropical and extratropical heat budget. The coupled model is run for 50 years under present-day orographic and albedo-conditions forced by different CO_2 concentrations (100, 200, 280, 560 and 700 ppm). A surface temperature equilibration in the Pacific takes place after about 20 years and only the last 30 years of the individual simulations are analyzed. The results are summarized in Fig. 15. The eastern equatorial Pacific (Fig. 15a) shows a rather linear response to the radiative forcing (proportional to the logarithm of the CO_2 concentrations). The square indicates the LGM state. It turns out that the CO_2 reduction between LGM and pre-industrial climate contributes only 20% to the total eastern equatorial Pacific cooling. This further highlights the importance of dynamical changes and atmosphere-ocean interactions for the LGM cooling. The situation in the northeastern Pacific (30–45°N, 160–130°W) is more complicated. The warming levels off at high CO_2 concentrations, possibly due to a dynamical thermostat effect. It is difficult to obtain northeastern temperatures higher than 1 °C, simply by increasing the CO_2 concentrations. However, the dynamical effect due to the orographically induced atmospheric circulation changes can easily lead to a warming of about 2 °C (square in Fig. 15b).

The results highlight the delicate balance between radiative cooling, ocean dynamical warming and the sensible and latent heat fluxes to control North Pacific temperatures.

7 The LGM: in the aftermath of Heinrich event 2

Very often, modelling studies assume that the LGM climate state is a stationary equilibrium state, which can be simulated realistically using long spin-up simulations and glacial boundary conditions. However, many of these studies neglect the fact that the LGM occurred about 2000–3000 years after the major meltwater pulse Heinrich 2 (Heinrich 1988). It is not clear whether the thermohaline circulation had recovered already at the time of the LGM, or whether the LGM climate is still in an unrecovered THC state. Here, for purposes of clarification we will pursue the extreme case of no recovery. In order to mimick such a situation an additional experiment is conducted using glacial boundary conditions and an anomalous meltwater forcing. A transient 400-year long simulation is conducted (Heinrich experiment) in which the freshwater input into the North Atlantic (40–60°N) is increased for about 400 years, following a Gaussian profile with a width of 400 years. The associated global sea-level rise amounts to about 8 m. Here we analyze the last 100 years of this simulation which are characterized by a collapsed THC state, as shown in Fig. 16. In comparison with Fig. 3 we see that a reduction of North Atlantic Deep-Water formation is associated with an enhanced export of Antarctic Bottom Water into the North Atlantic. Furthermore, one observes an enhancement of the thermocline circulation in the Northern Hemisphere. These circulation changes are associated with large-scale anomalies of the divergence of the heat transport and hence help to generate SST changes, in particular in the North Atlantic region. These diabatic forcing anomalies in turn have an impact on the mean atmospheric circulation, as shown in Fig. 17. The collapsed THC state triggers a wave number 1 pattern in the upper levels of the atmosphere. The upper level geopotential height anomalies between the Heinrich experiment and the LGM simulation attain values similar to those triggered by the

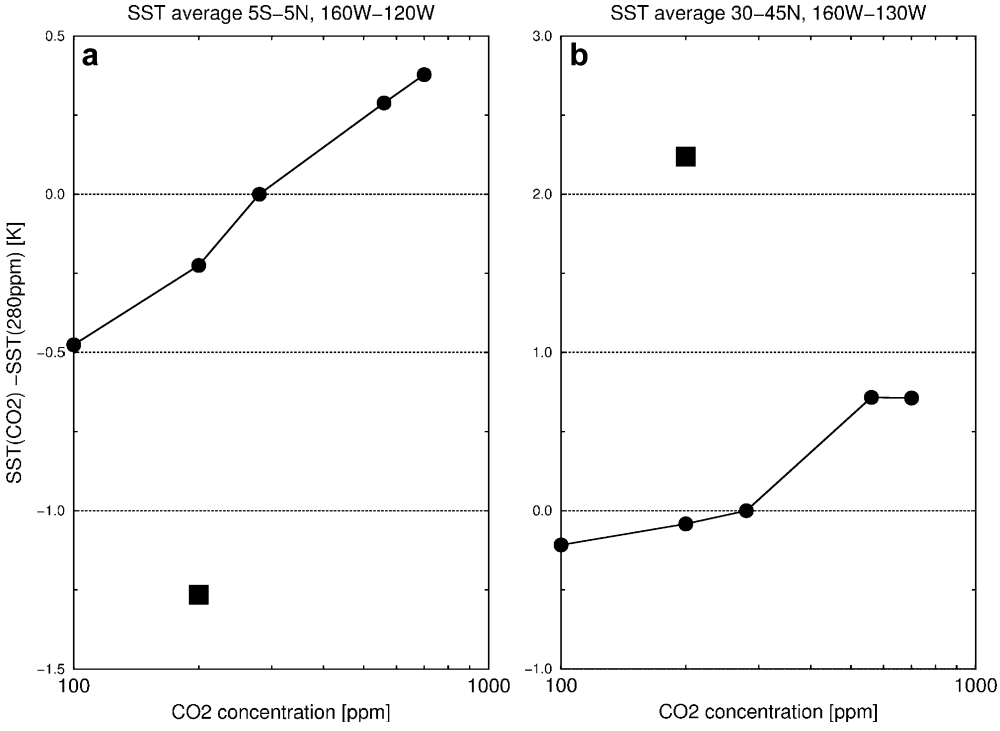

Fig. 15 **a** Averaged eastern equatorial Pacific temperatures anomalies for different atmospheric CO_2 concentrations (*circles*) and for the LGM simulation (*square*) **b** Same as left but for the northeastern Pacific

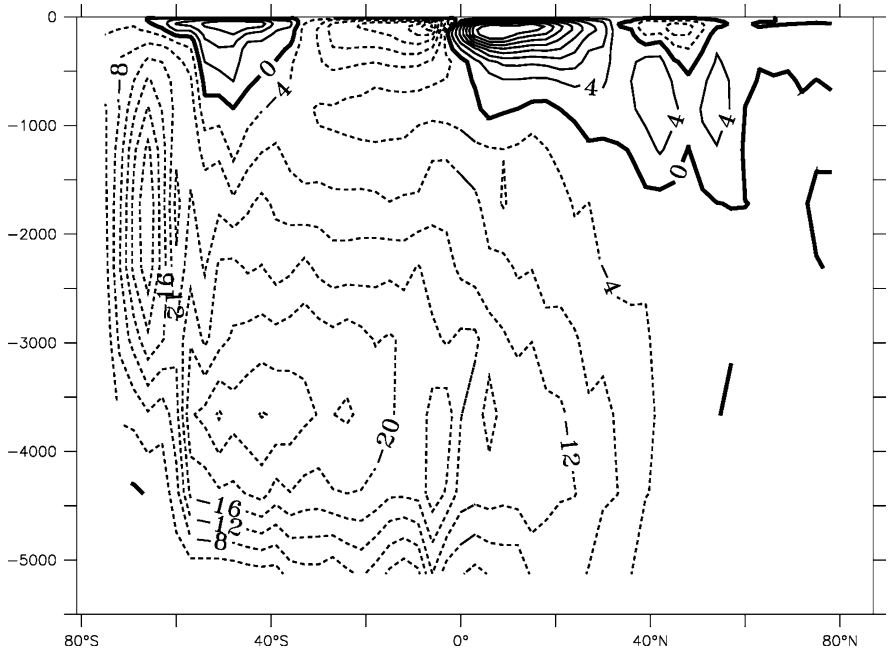

Fig. 16 Time average (years 300–400) of the zonally averaged global stream function (Sv = 10^6 m^3/s) Heinrich LGM simulation

glacial orographic forcing. In lower levels, however the amplitude of the anomalies is strongly diminished, thereby forming an equivalent barotropic response. The wind anomalies will lead to an intensfied cold-air advection in the subpolar North Pacific area. The simulated SST difference between the Heinrich and the LGM simulation, as displayed in Fig. 18, reveals a cooling of the subpolar North Pacific and a significant warming in the area of the Antarctic Circumpolar Current and the subtropical southern Pacific which originates from the bipolar see-saw effect (Blunier et al. 1998; Clark et al. 2002). Both tendencies will help to enhance the degree of similarity between the CLIMAP SST anomaly pattern and the post-Heinrich event LGM climate state. Further details on the Heinrich simulations will be presented in a forthcoming study.

8 Summary and discussion

The aim of this study was to disentangle the mechanisms that are responsible for glacial surface temperature

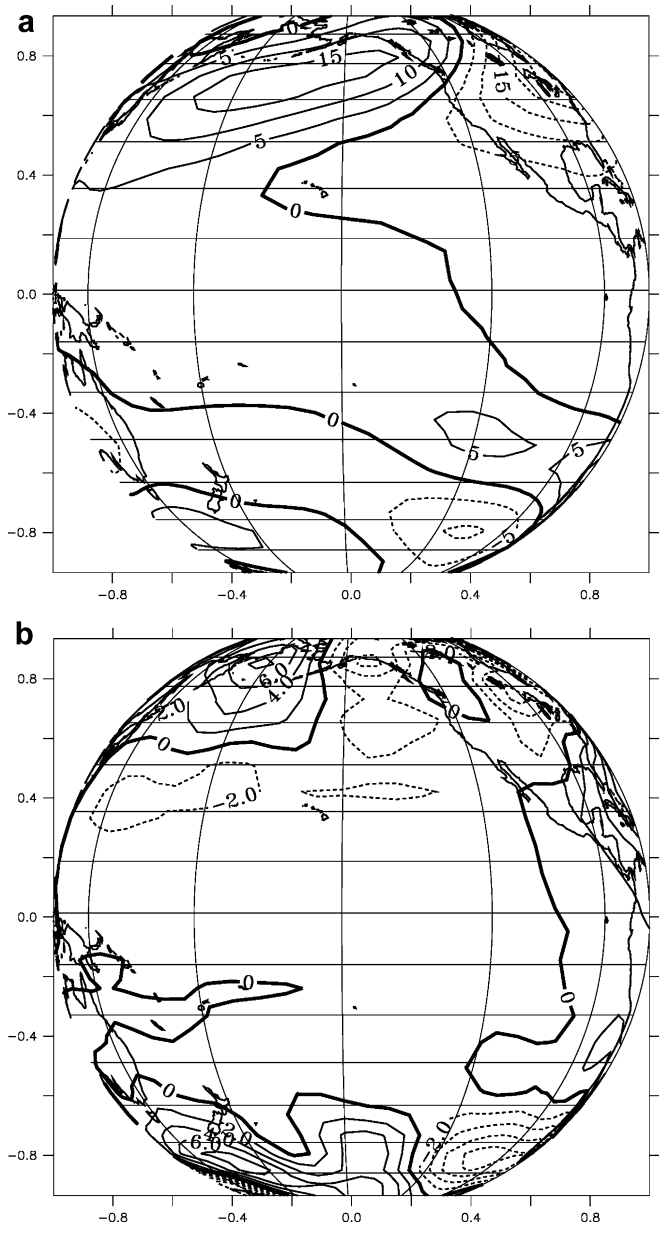

Fig. 17 Annual mean eddy geopotential height difference (m) between Heinrich and LGM simulation **a** at 200 hPa and **b** at 800 hPa

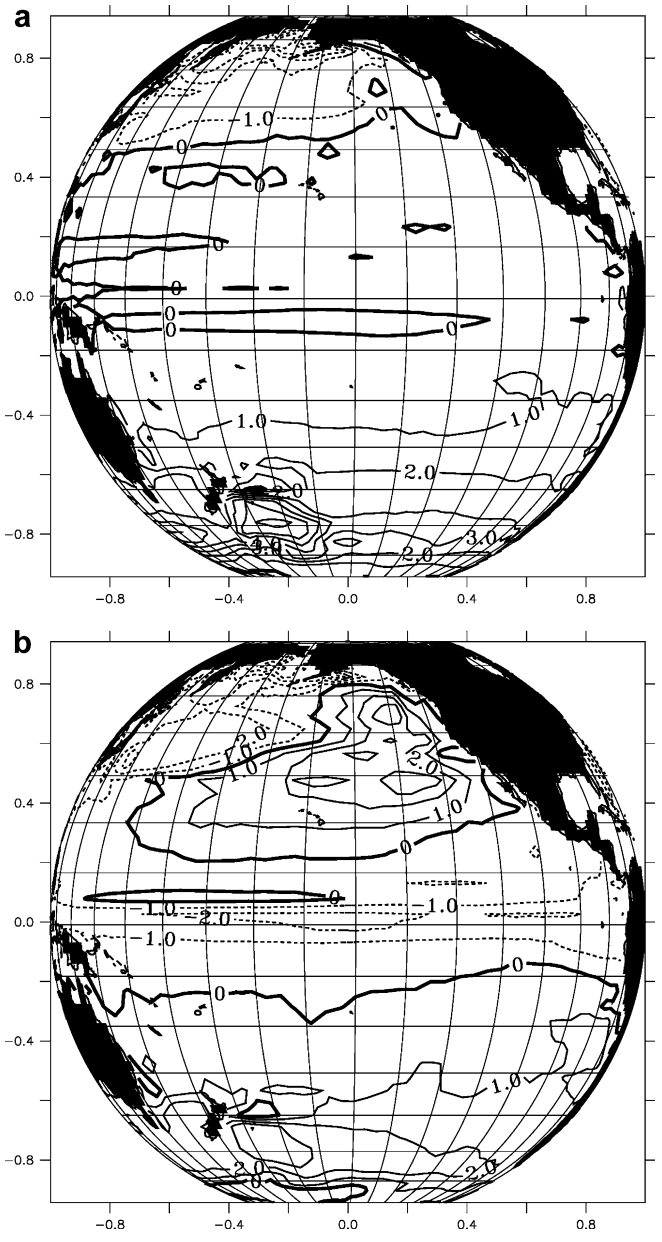

Fig. 18 **a** Sea surface temperature anomalies (K) computed from the difference between Heinrich and LGM simulation. **b** SST change between Heinrich and CTR simulation (K)

changes in the North Pacific. The analysis is based on a series of multi-centennial coupled model simulations that are performed with the coupled model of intermediate complexity ECBILT/CLIO (version 3.0). The equilibration time of surface temperatures and currents in the Pacific is short (less than 30 years) as compared to the adjustment of the North Atlantic (about 300 years). The simulated difference between the Pacific SST pattern during the LGM and the pre-industrial control simulation bears many similarities with the SSTA reconstruction of CLIMAP (1981). Both, in the simulation and in the reconstruction a northeastern Pacific warming can be observed, which exhibits a strong seasonal modulation (not shown). We argue that zonal mean wind changes over the Pacific drive anomalous orographically forced stationary wave patterns (Fig. 8), which in turn lead to a reduction of latent and sensible ocean cooling in the subtropical Pacific (see Fig. 14). The weakening of the westerlies leads to an enhanced warming of the northeastern Pacific.

Two other processes are identified that contribute to the simulated North Pacific warming: The orographically forced stationary wave pattern (Fig. 8) is associated with a reduction of the mean wind-stress curl over the Kuroshio area. This leads to a spin-down of the subtropical and the subpolar gyre, as diagnosed from the Sverdrup transport relationship (not shown). As a consequence of the wind-induced transport anomalies,

the Kuroshio area cools down, whereas the northeastern Pacific warms up (Fig. 14). This generates a typical dipole-like pattern between western and eastern Pacific, which can be identified also in the CLIMAP (1981) reconstruction. The other mechanism that contributes to the North Pacific warming (Fig. 4) is based on remote tropical forcing. The permanent La Niña-type pattern induces an anomalous atmospheric circulation which encompasses also the North Pacific. Since the teleconnection patterns for a permanent La Niña state are very much the same as those for an interannual La Niña state (due to the fast adjustment time of the atmosphere) we are able to diagnose a tropical extratropical atmospheric bridge. It is provided by an equatorially forced stationary wave pattern (Fig. 6) which blocks zonal flow over the northeastern Pacific and North America. This large-scale blocking situation which is also typical for a present-day La Niña state generates a North Pacific surface warming between 20–40°N due to a reduction of the wind-strength, and latent and sensible heat fluxes (Fig. 6).

In addition, we studied the physical origin of the simulated tropical cooling: changes in the orographically induced waves lead to an eddy momentum flux convergence in the upper troposphere near 30°N. The Kuo-Eliassen equation (Kuo 1956) predicts that upper level momentum flux convergence will create an anomalous indirect circulation with ascending motion to the south of the convergence and descending motion to the north of it. This anomalous vertical circulation enhances the surface pressure gradient between 15–35°N, thereby driving stronger surface easterlies. In turn the intensification of the trade winds by about 30% leads to a spin-up of the subtropical cell by Ekman transport. A stronger subtropical cell leads to stronger equatorial upwelling and eventually to colder surface temperatures.

Parts of this feedback chain were identified using standard diagnostic tools. What remains unresolved are the detailed processes which lead to an enhancement of eddy momentum fluxes in the atmosphere. The eddy momentum flux anomalies can be partly (50%) attributed to a change in orographically induced stationary waves and to an increase in transient wave activity which results mainly from an enhanced thermal gradient over the ice-sheets. A detailed description of the atmospheric changes will be given in a forthcoming study.

Two other processes are important in controlling oceanic surface temperatures during the last glacial period. Local radiative forcing due to reduced CO_2 concentrations and reduced humidity in the atmosphere contribute to an overall cooling. However, compared to the ocean dynamical changes, this local forcing is relatively weak in our coupled model (Fig. 15). Furthermore, the state of the North Atlantic THC determines also temperatures in the subpolar North Pacific as well as in the subtropical South Pacific due to oceanic and atmospheric connections. Due to the uncertainty in the determination of the THC state during the LGM, this effect may modulate Pacific temperatures significantly.

The underestimation of zonal temperature gradients in the tropics might be an important caveat of our model which may modify the LGM climate response in the tropical Pacific. Further studies will elucidate whether the physical mechanisms diagnosed from our intermediate complexity model are robust. It has to be noted here, that e.g. the LGM simulation performed with the NCAR CSM (Shin et al. 2003) exhibits an enhancement of the subtropical gyre transports during the LGM, in contrast to our model simulation. This indicates that LGM wind-stress changes over the Pacific area and their implications for the oceanic surface heat budget are probably also strongly model-dependent.

Keeping in mind the discrepancies between LGM simulations performed with different CGCMs, it is even more difficult to compare climate model results directly with paleo reconstructions of surface temperatures. There are only very few data from the central North Pacific ocean which can be regarded as reliable SST proxies. Sediment cores from around the Hawaiian Islands (Hostetler and Mix 1999) may be unrepresentative for the central North Pacific, because of island-specific effects. In particular, the island wake effect (Xie et al. 2001) may contaminate SST reconstructions from the Hawaiian Islands by several tenths of a degree. The island wake effect is strongly modulated by the strength of the trade winds, creating a wind-stress curl near the Hawaiian Islands. In turn this curl pushes warm western Pacific waters into the area of the wake. The atmosphere responds to these SST anomalies by amplifying the curl and hence the SST anomalies by a few tenths of degrees. This implies that the trade winds which were considerably stronger during the LGM (Andreasen and Ravelo 1997; Liu et al. 2000) strongly modify the SST west of the Hawaiian Islands, where some of the sediment cores for the LGM have been taken (Lee and Slowey 1999). Therefore, it remains unclear whether Hawaiian SST proxies really represent temperatures of the open central Pacific. In addition, there is also an uncertainty in SST reconstructions based on Hawaiian snow lines (see Crowley 2000 for a discussion). Assuming a constant atmospheric lapse rate these reconstructions suggest much colder sea surface temperatures during the LGM, as inferred from marine proxies. Still unclear is the validity of the assumption of constant lapse rates (Sun and Lindzen 1993) and whether the snow lines represent only a surface temperature changes. They may also reflect partly changes in large-scale precipitation patterns. In fact, our LGM experiment simulates much higher precipitation rates in the subtropical North Pacific, owing to the positive SST anomalies. In altitudes of about 3000–4000 m (Mauna Kea) such changes may lead also to a depression of the snow lines.

To summarize briefly, there is both a considerable modelling and LGM-data uncertainty. In particular, the subtropical North Pacific LGM SST anomalies seem to depend on the details of the coupled model, as well as on the reconstruction techniques. In the tropical Pacific on the other hand, modelling results and SST reconstruc-

tions seem to converge far better than in the subtropics. The coupled climate models, used for LGM experiments (Bush and Philander 1998; Shin et al. 2003; Hewitt et al. 2001; Kitoh et al. 2001; Kim et al. 2003) show a rather homogenous cooling throughout the tropical oceans by about 2–5 °C. Cooling in the tropical Pacific can be found also in latest temperature reconstructions (Hostetler and Mix 1999; Andreasen and Ravelo 1997; Crowley 2000; Farrera 1999; Kerr 1995; Lee and Slowey 1999; Pisias and Rea 1988; Koutavas et al. 2002). The details of the east-west structure of this equatorial Pacific cooling are, however, still controversial (see Koutavas et al. 2002; Liu et al. 2000).

We have shown that North Pacific temperature anomalies during the LGM originate from a delicate balance between different physical processes, namely radiative forcing due to CO_2 and water vapor reduction, large-scale ocean-dynamical changes which are triggered by glacial wind anomalies and a tropical-extratropical bridge forced by tropical SST anomalies.

The relative importance of these processes are certainly model-dependent and this could explain why the simulated temperature changes can be so different between different models. The goal of our study was to determine important physical processes which contribute to the simulated LGM cooling in the tropics and the warming in the northeastern Pacific. We did not aim to find a definite answer on their relative contributions.

Our results have underlined the importance of the North Pacific during the LGM as a test case for understanding processes driving Earth's climate. When better estimates of SST are available, it should be possible to check the relative influence of critical processes such as the teleconnection from the tropics and the response of SST to local wind changes as well as their representation in models.

Acknowledgements This work is supported by the Deutsche Forschungsgemeinschaft (DFG) through the Collaborative Research Project SFB460 and CAPES-Brasilia, Grant 0794023. We thank Dr. A. Bush and an anonymous reviewer for their help comments on this work.

References

Andreasen D, Ravelo A (1997) Tropical Pacific Ocean thermocline depth reconstructions for the last glacial. Paleoceanography 12: 395–414

Bjerknes J (1969) Atmospheric teleconnections from the equatorial Pacific. Mon Weather Rev 97: 163–172

Blunier T, Chappellaz J, Schwader J, Dällenbach A, Stauffer B, Stocker T, Raynaud D, Jouzel J, Clausen H, Hammer C, Johnsen S (1998) Asynchrony of Antarctica and Greenland during the Last Glacial. Nature 394: 739–743

Broccoli A, Manabe S (1987) The influence of continental ice, atmospheric CO_2 and land albedo on the climate of the last glacial maximum. Clim Dyn 1: 87–99

Bush A (2001) Simulating climates of the last glacial maximum and of the mid-holocene: wind changes, atmosphere-ocean interactions, and the tropical thermocline. AGU Monograph series (Oceans and rapid past and future climate changes: North-South connections)

Bush ABG, Philander SGH (1998) The role of ocean-atmosphere interactions in tropical cooling during the last glacial maximum. Science 279: 1341–1344

Campin J, Goosse H (1999) A parameterization of dense overflow in large-scale ocean models in z coordinate. Tellus 51A: 412–430

Clark P, Pisias N, Stocker T, Weaver A (2002) The role of the thermohaline circulation in abrupt climate change. Nature 415: 863–869

CLIMAP (1981) Seasonal reconstruction of the Earth's surface of the last glacial maximum. Geol Soc Am Map Chart Ser, MC-36: 1–18

Cook K, Held I (1988) Stationary waves of the ice age climate. J Clim 1: 807–819

Crowley T (2000) ClLMAP SSTs re-revisited. Clim Dyn 16: 241–245

Crowley T, Baum S (1997) Effect of vegetation on an ice-age climate model simulation. J Geophys Res 102: 16,463–16,480

Farrera I (1999) Tropical palaeoclimates at the last glacial maximum: a new synthesis of terrestrial data. Clim Dyn 15: 823–856

Gent P, McWilliams J (1990) Isopycnal mixing in ocean general circulation models. J Phys Oceanogr 20: 150–155

Goosse H, Fichefet T (1999) Importance of ice-ocean interactions for the global ocean circulation: a model study. J Geophys Res 104(C10):23,337–23,355

Goosse H, Deleersnijder E, Fichefet T, England M (1999) Sensitivity of a global coupled ocean-sea ice model to the parameterization of vertical mixing. J Geophys Res 104(C6): 13,681–13,695

Goosse H, Selten F, Haarsma R, Opsteegh J (2002) Large sea-ice volume anomalies simulated in a coupled climate model. Clim Dyn 10, DOI: 10.1007/s00382-002-0290-4

Guilderson T, Fairbanks R, Rubenstone J (1994) Tropical temperature variations since 20 000 years ago: modulating interhemispheric climate change. Science 263: 663–665

Heinrich H (1988) Origin and consequences of cyclic ice rafting in the North West Atlantic Ocean during the past 130 000 years. Quat Res 29: 143–152

Held I, Suarez M (1978) A two-level primitive equation atmosphere model designed for climate sensitivity experiments. J Atmos Sci 35: 206–229

Hewitt CD, Broccoli A, Mitchell J, Stouffer RJ (2001) A coupled model of the last glacial maximum: was part of the North Atlantic relatively warm? Geophys Res Lett 28: 1571–1574

Hostetler S, Mix A (1999) Reassessment of ice-age cooling of the tropical ocean and atmosphere. Nature 399: 673–676

Houghton EJT, Ding Y, Griggs D, Noguer M, Linden PV, Dai X, Maskell K, Johnson CA (eds) (2001) Climate change 2001. The scientific basis. Cambridge University Press, Cambridge, UK, pp 881

Jones PD (1994) Hemispheric surface air temperature variations: a reanalysis and an update to 1993. J Clim 7: 1794–1802

Kerr R (1995) Chilly ice-age tropics could signal climate sensitivity. Science 267: 961

Kim S, Flato G, Boer G (2003) A coupled climate model simulation of the last glacial maximum, part 2: approach to equilibrium. Clim Dyn 20: 635–661

Kitoh A, Muakami S, Koide H (2001) A simulation of the last glacial maximum with a coupled atmosphere-ocean GCM. Geophys Res Lett 28: 2221–2224

Klinger B, McCreary J, Kleeman R (2002) The relationship between oscillating subtropical wind stress and equatorial temperature. J Phys Oceanogr 32: 1507–1521

Knutson T, Manabe S, Gu D-F (1997) Simulated ENSO in a global coupled ocean-atmosphere model: multi-decadal amplitude modulation and CO_2 sensitivity. J Clim 10: 138–161

Kohlfeld K, Harrison S (2000) How well can we simulate past climates? Evaluating the models using palaeo-environmental datasets. Quat Sci Rev 19: 321–346

Koutavas A, Lynch-Stieglitz J, Marchitto JT, Sachs J (2002) El Niño-like pattern in ice age tropical Pacific sea surface temperature. Science 297: 226–230

Kuo H (1956) Forced and free meridional circulations in the atmosphere. J Meteorol 13: 561–568
Lau N, Nath M (1996) The role of the "atmospheric bridge" in linking tropical Pacific ENSO events to extratropical SST anomalies. J Clim 9: 2036–2057
Lea D, Pak DK, Spero HJ (2000) Climate impact of late Quaternary Equatorial Pacific sea surface temperature variations. Science 289: 1719–1724
Lee K, Slowey N (1999) Cool surface waters of the subtropical north Pacific during the last glacial. Nature 397: 512–514
Liu Z, Kutzbach J, Wu L (2000) modelling climate shift of El Niño variability in the Holocene. Geophys Res Lett 27: 2265–2268
Liu Z, Philander S (1995) How different wind stress patterns affect the tropical-subtropical circulations of the upper ocean. J Phys Oceanogr 25: 449–462
Liu Z, Shin S, Otto-Bliesner B, Kutzbach J, Brady E (2002) Enhanced tropical cooling at the last glacial maximum by extratropical ocean ventilation. Geophys Res Lett 29, doi:10.1029/2001GL013938
Marshall J, Molteni F (1993) Toward a dynamic understanding of planetary-scale flow regimes. J Atmos Sci 50: 1792–1818
McCreary J, Lu P (1994) Interaction between the subtropical and the equatorial ocean circulations: the subtropical cell. J Phys Oceanogr 24: 466–497
Mellor G, Yamada T (1982) Development of a turbulence closure model for geophysical fluid problems. Rev Geophys Space Phys 20: 851–875
Oberhuber JM (1988) An atlas based on 'COADS' data set Tech Rep 15, Max Planck Institut für Meteorologie, Hamburg, Germany
Opsteegh J, Haarsma R, Selten F, Kattenberg A (1998) ECBILT: A dynamic alternative to mixed boundary conditions in ocean models. Tellus 50A: 348–367
Peltier W (1994) Ice age paleotopography. Science 265: 195–201
Pflaumann U, Sarnthein M, Chapman M, D'Abreu L, Funnell B, Huels M, Kiefer T, Maslin M, Schulz H, Swallow J, van Kreveld S, Vautravers M, Vogelsang E, Weinelt M (2003) Glacial North Atlantic: sea-surface conditions reconstructed by GLAMAP 2000. Paleoceanography 18: 1065, doi: 10.1029/2002PA000774
Pisias N, Mix A (1997) Spatial and temporal oceanographic variability of the eastern equatorial Pacific during the late Pleistocene: evidence from radiolaria microfossils. Paleoceanography 12: 381–393
Pisias N, Rea R (1988) Late Pleistocene paleoclimatology of the central equatorial Pacific: sea surface response to the southeast trade winds. Paleoceanography 3: 21–38
Porter S (1979) Hawaiian glacial climates. Quat Res 12: 161–187
Rind D (1987) Components of the ice age circulation. J Geophys Res 92: 4241–4281
Rind D, Peteet D (1985) Terrestrial conditions at the last glacial maximum and CLIMAP sea-surface temperature estimates, are they consistent? Quat Res 24: 1–22
Sarnthein M, Pflaumann U, Weinelt M (2003) Past extent of sea ice in the northern North Atlantic inferred from foraminiferal paleotemperature estimates. Paleoceanography 18: 1047, doi:10.1029/2002PA000771
Shin SI, Liu Z, Bliesner BLO, Kutzbach EB, Kutzbach JE, Harrison SP (2003) A simulation of the last glacial maximum climate using the NCAR CSM. Clim Dyn 20: 127–151
Stute M, Forster A, Frishkorn A, Serejo J, Clark R, Schlosser P, Broecker W, Bonani G (1995) Cooling of tropical Brazil (5 °C) during the last glacial maximum. Science 269: 379–383
Sun D, Lindzen R (1993) Water vapor feedback and the ice age snow line record. Ann Geophysicae 11: 204–215
Timmermann A, Latif M, Voss R (1999) Modes of climate variability as simulated by the coupled atmosphere-ocean model ECHAM3/LSG, Part 1: ENSO-like climate variability and its low-frequency modulation. Clim Dyn, 15: 605–618
Xie S, Liu W, Liu Q, Nonaka M (2001) Far-reaching effects of the Hawaiian islands on the Pacific ocean-atmosphere. Science 292: 2057–2060